RESEARCH ARTICLE

Key Points:
- We are able to simulate δ^{18}O in three time slices during the LIG, discovering seasonal dependencies in the isotopic responses
- Comparing our simulation to ice core records indicates a generally good agreement of δ^{18}O values
- We find that the spatial δ^{18}O relationship cannot reconstruct temporal differences when small magnitude temperature changes are considered

Supporting Information:
- Supporting Information S1
- Table S1

Correspondence to:
P. Gierz,
pgierz@awi.de

Simulating climate and stable water isotopes during the Last Interglacial using a coupled climate-isotope model

Paul Gierz[1] , Martin Werner[1] , and Gerrit Lohmann[1]

[1]Helmholtz Center for Polar and Marine Research, Alfred Wegener Institute, Bremerhaven, Germany

Abstract Understanding the dynamics of warm climate states has gained increasing importance in the face of anthropogenic climate change, and while it is possible to simulate warm interglacial climates, these simulated results cannot be evaluated without the aid of geochemical proxies. One such proxy is δ^{18}O, which allows for inference about both a climate state's hydrology and temperature. We utilize a stable water isotope equipped climate model to simulate three stages during the Last Interglacial (LIG), corresponding to 130, 125, and 120 kyr before present, using forcings for orbital configuration as well as greenhouse gases. We discover heterogeneous responses in the mean δ^{18}O signal to the climate forcing, with large areas of depletion in the LIG δ^{18}O signal over the tropical Atlantic, the Sahel, and the Indian subcontinent, and with enrichment over the Pacific and Arctic Oceans. While we find that the climatology mean relationship between δ^{18}O and temperature remains stable during the LIG, we also discover that this relationship is not spatially consistent. Our results suggest that great care must be taken when comparing δ^{18}O records of different paleoclimate archives with the results of climate models as both the qualitative and quantitative interpretation of δ^{18}O variations as a proxy for past temperature changes may be problematic due to the complexity of the signals.

1. Introduction

With the increasing concern over the possible extent of anthropogenically caused global warming, there has been a corresponding increase in demand for more rigorous climate model evaluation. While general circulation models of the Earth's climate are generally tuned and evaluated against present day conditions [*Knutti et al.*, 2010], testing the ability of climate models to accurately reproduce the climate of the past extends this evaluation one step further, allowing for a more robust understanding of the models' skill in simulating any number of complex climate scenarios [*Lohmann et al.*, 2013a]. Model intercomparisons of warm climates, both on longer time scales of several million years, such as the Pliocene [*Haywood et al.*, 2013], as well as for more recent warm periods during the Quaternary, such as the Holocene [*Bakker et al.*, 2014] or Marine Isotope Stage (MIS) 5.5e [*Bakker et al.*, 2013; *Lunt et al.*, 2013], allow us to test how well a model can generally reproduce warm climates under external forcing and the resulting internal feedbacks.

Model-data comparisons for various paleoclimates have generally been quite successful in past studies [*Braconnot et al.*, 2012; *Lohmann et al.*, 2013a; *Pfeiffer and Lohmann*, 2016]. However, since direct measurements of key climate variables such as temperature and precipitation are only available on a global scale for the last $\approx$130 years, paleoclimatology must rely on geochemical proxies to allow for the reconstruction of the climate state in the past; which necessitates the conversion of isotopic or chemical element ratios to climate variables like temperature or precipitation amount, a method subject to calibration and potential errors. More recently, paleoclimate modeling studies have begun to adopt a new method, enabling the climate models to directly simulate paleoclimate proxies.

2. Stable Water Isotopes as a Climate Proxy

One example of a highly relevant geochemical climate proxy is the various stable isotopes of water, H_2O, $H_2^{18}O$, and $^1H^2HO$ (also referred to as HDO). These stable water isotopes, and the mechanisms by which they fractionate and distribute throughout the various hydrological reservoirs of the climate system, have provided a powerful tool for reconstructing past climate situations [*Dansgaard*, 1964]. In particular, these stable

water isotopes (hereafter referred to via a usual δ-notation with respect to the Vienna Standard Mean Ocean Water, V-SMOW) have been used to make inferences about past temperatures and precipitation. δ^{18}O and δD trapped in polar ice cores have been used for past temperature reconstructions over interglacial-glacial cycles [*EPICA Community Members*, 2004]. Subtropical isotope archives, such as speleo-thems, have been employed to provide an indication of the amount of precipitation via the water isotope composition [*Drysdale et al.*, 2004, 2009]. While it is possible to measure the isotopic composition of past precipitation in some archives directly, e.g., in ice cores, other archives necessitate a transfer function from the isotopic composition of the ambient water to the ultimately preserved isotope signal in the climate archive, e.g., as it is the case for the δ^{18}O records of calcite shells from marine species such as fora-minifera [*Kim et al.*, 2006].

To quantitatively transfer water isotope variations into changes of temperature or precipitation amount, a necessary assumption must be made a priori, namely, that during variations of a climate state, both tempo-rally and spatially, a constant relationship between changes of the climate variable and the variability of the recorded isotopic signal is maintained. If we aim to better understand possible future warmer-than-present climate scenarios by examining past warm periods, a necessary first step will be to test if the temperature-isotope relationship has stayed constant in time and space in both the preindustrial climate and past warm interglacials. For δ^{18}O in precipitation and surface temperatures (t_a), this relationship was first reported by *Dansgaard* [1964], and the following linear dependency between δ^{18}O and t_a on the global spatial scale was found:

$$\delta^{18}\text{O} = 0.69 t_a - 13.6\text{\textperthousand}$$

Here the linear factor $0.69\text{\textperthousand}/°$C was empirically derived from a global data set provided by GNIP (Global Network of Isotopes in Precipitation) [*IAEA/WMO*, 2017]. On a regional scale, the value of the δ^{18}O-t_a-gradi-ent may vary, e.g., more recent studies report values of $0.8\text{\textperthousand}/°$C for both Greenland [*Masson-Delmotte et al.*, 2011] and Antarctica [*Masson-Delmotte et al.*, 2008].

3. The Last Interglacial

The Last Interglacial (LIG), spanning from 130 kyr before present (ka B.P.) to 115 ka B.P., has recently gained interest as it represents one of the climate's more stable warm states. Therefore, the paleoclimate commu-nity has been focusing on extending transient records to capture this climate period [*NEEM Community Members*, 2013]. During the LIG, the climate was generally warmer than present and data compilations made available by the *CAPE Last Interglacial Project Members* [2006] and, more recently, by *Capron et al.* [2014], suggest temperature changes ranging from $+4$ to $+5$°C. However, there is still some debate regard-ing the magnitude of this warming [*Bakker et al.*, 2013; *Otto-Bliesner et al.*, 2013; *Pfeiffer and Lohmann*, 2016] as the observational basis for the temperature reconstructions of the LIG rests often upon proxy data sets of either low temporal resolution or short duration. In addition to a general warming of the LIG, high-resolution proxies, such as those captured by fossilized corals [*Felis et al.*, 2004, 2015; *Brocas et al.*, 2016], suggest that the seasonal amplitude of temperature during the LIG was enhanced compared to the present day in the tropical North Atlantic. Additionally, global sea level may have been up to 7–8 m higher than pre-sent day [*O'Leary et al.*, 2013; *Dutton et al.*, 2015]. It is also possible that the geometry of the large continen-tal ice sheets both in Greenland [*Cuffey and Marshall*, 2000] as well as over Antarctica may have been different during the LIG, and some investigations regarding ice sheet geometry changes has been the sub-ject of recent model studies [*Sutter et al.*, 2016].

Our study aims to provide insight into the LIG by using a fully coupled climate model enhanced by explicit water isotope diagnostics. First, we examine the simulated climate state, as well as the modeled isotopic signatures of δ^{18}O during the LIG. Next, we examine the simulated δ^{18}O signals in relation to measurements from different archives in order to provide some insight into our model's ability to reproduce the measure-ments. We proceed to examine how far the modern spatial global δ^{18}O-T relationship described by *Dans-gaard* [1964] may be found for the LIG climate, too. Finally, we analyze if global and selected regional δ^{18}O-T relationship may vary during the LIG, and if LIG changes of δ^{18}O can be always converted into LIG changes of surface temperatures in a consistent manner.

4. Model Description and Experimental Design

All simulations of this study have been performed using the Earth system model ECHAM5/MPIOM [*Jungclaus et al.*, 2006], enhanced by a stable water isotope diagnostic. The model, which is fully documented in *Werner et al.* [2016], consists of the atmospheric model ECHAM5-wiso [*Werner et al.*, 2011], the dynamic vegetation module JSBACH-wiso [*Haese et al.*, 2013], and the ocean/sea-ice module MPIOM-wiso [*Xu et al.*, 2012]. A brief description of each model component follows.

The atmospheric model ECHAM5-wiso utilizes a resolution of T31L19, corresponding to roughly 3.75° × 3.75° laterally, and 19 vertical levels [*Roeckner et al.*, 2006]. Vertically, the model is resolved along hybrid sigma topography following coordinates, with exponentially widening of level spacing in the upper atmosphere. The model uses a spectral solution for the equations of state describing the physical conservation of mass, energy, and momentum. ECHAM5-wiso simulates a full hydrological cycle within the atmosphere, including evapotranspiration of terrestrial water, as well as evaporation from the ocean. Cloud simulation in ECHAM5-wiso is based on two different schemes for large-scale and convective clouds. Within the model's hydrological cycle, tracers for stable water isotopes are included allowing for a full, dynamic simulation of $H_2^{18}O$ and HDO, along with fractionation changes between the various sources and sinks [*Werner et al.*, 2011].

The vegetation module JSBACH-wiso not only simulates dynamic vegetation changes in respond to various climate conditions but also contains an implementation of a full water cycle and its isotopic variations within this vegetation module [*Haese et al.*, 2013]. JSBACH-wiso simulates eight vegetation types, referred to as Plant Functional Types (PFTs) and implements water reservoirs for snow coverage, soil water, and water within the plant's skin layer. Further details about the vegetation module can be found in *Brovkin et al.* [2009].

The ocean/sea-ice model MPIOM simulates ocean dynamics and sea-ice formation processes in the ocean [*Jungclaus et al.*, 2006]. MPIOM-wiso, documented by *Xu et al.* [2012] extends this model with stable water isotope distributions. In this study, we utilize a bipolar grid with model poles over Greenland and Antarctica with a resolution of GR30, corresponding to a horizontal resolution of approximately 3.5° × 1.5° laterally, with a higher resolution at the model's poles. Vertically, the MPIOM-wiso setup contains 40 unevenly spaced layers, with higher resolution at the ocean's surface. MPIOM-wiso is able to simulate sea-ice formation, transport, and melting, along with isotope compositions in the ice.

We simulate three time slices during the LIG, corresponding to 120, 125, and 130 ka B.P., prescribing both greenhouse gas (GHG) and orbital forcings as recommended by the PMIP protocol. We refer to these experiments as LIG-120, LIG-125, and LIG-130, respectively. Additionally, we perform a control simulation using preindustrial (PI) forcing. The values for the orbital parameters were derived based upon the *Berger and Loutre* [1991] solution, and the PMIP GHG forcings are based on data extracted from Antarctic ice cores. The values are set according to *Lüthi et al.* [2008] for CO_2, *Loulergue et al.* [2008] for CH_4, and *Spahni et al.* [2005] for N_2O. Dynamic vegetation is started with PI values and allowed to adapt to the climate state for each time slice. We do not modify the global $\delta^{18}O$ and δD budget for the water isotopes, as we assume a PI ice sheet configuration in all experiments and do not modify the global sea level. All time slices underwent long-term spin-ups of 3000 years, followed by an evaluation period of 100 years used for analysis. The simulations are summarized in Table 1.

To ensure that the simulations are in equilibrium after the spin-up period, we examine the trends in the global deep ocean salinity and isotopic composition. The globally averaged deep ocean salinity changes by less than 0.01% over 100 years, corresponding to salinity changes that are less than 0.002 practical salinity

Table 1. Orbital and Greenhouse Gas Forcings Used for LIG Experiments

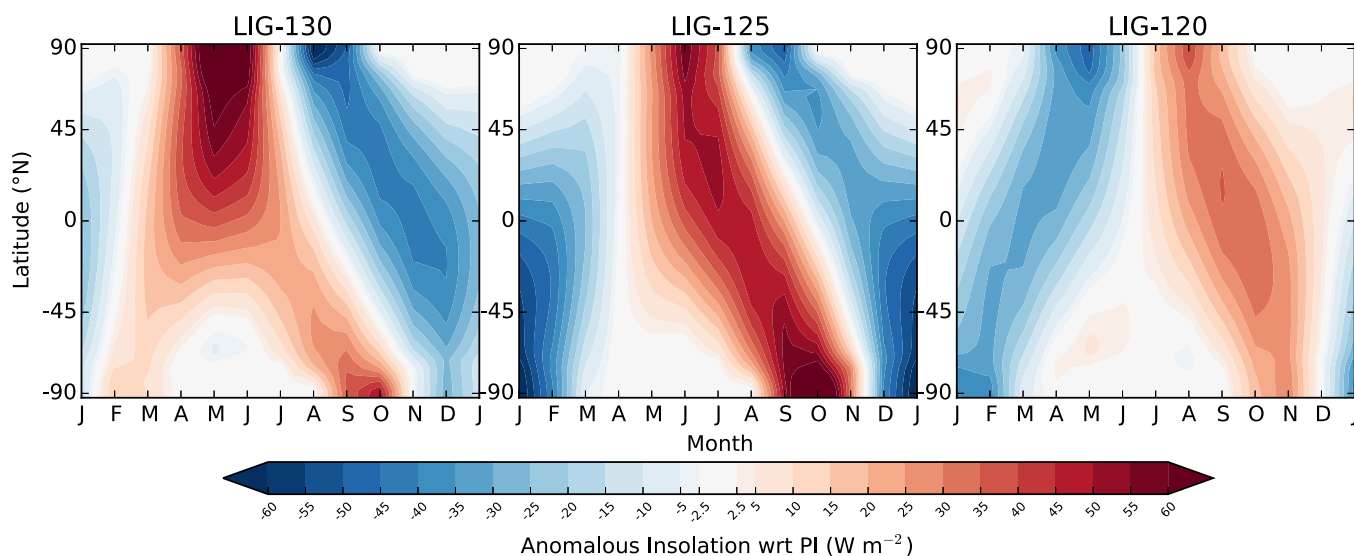| Experiment	CO$_2$	CH$_4$	NO$_2$	Eccentricity	Obliquity	Precession
PI	280	760	270	0.016724	23.446	282.04
LIG-120	268	572	261	0.041090	22.998	209.04
LIG-125	276	640	263	0.040000	23.790	127.14
LIG-130	257	512	238	0.038209	24.246	48.320

Figure 1. Changes in incoming solar radiation with respect to PI as a result of the modified orbital configurations for each of the three time slices LIG-130, LIG-125, and LIG-120. Due to the strong obliquity forcing in LIG-130 and LIG-125, a substantial seasonal signal can be seen, particularly in the high latitudes.

units (psu) in magnitude, and the globally averaged δ^{18}O signature of the deep ocean changes by less than 0.002‰.

The LIG is primarily forced by changes in the orbital configuration. As such, it is to be expected that any changes to the surface temperature (ST) are controlled by a related change in the atmospheric insolation and the resulting climate feedbacks. We present the prescribed changes to the incoming solar radiation distribution throughout the year in Figure 1. As compared to the PI time period, we see an increase in incoming solar radiation in boreal summers for LIG-130 and LIG-125 over the Northern Hemisphere, and a decrease in radiation in fall. Over the Southern Hemisphere, the insolation increase happens later in the year, between September and November. LIG-120 presents a very different pattern, with a decrease in insolation during the first half of the year, and an increase in the second half.

5. Results and Discussion

We divide our discussion into several parts, first presenting and discussing changes in surface temperatures and precipitation amounts and possible reasons for these changes, and comparing these changes to other simulations of the LIG where possible. Following this, we discuss the simulated changes in the isotopic composition of precipitation, and compare these simulated isotopic values to measurements of Greenland and Antarctic ice cores as well as several speleothem records. Thereafter, we conclude our discussion by examining the stability of the δ^{18}O-temperature relationship to understand the extent to which this relationship may be utilized as a paleothermometer.

5.1. Changes in Physical Responses: Surface Temperature

Simulated yearly mean surface temperature changes are shown in Figure 2. The climatologically averaged temperature responses in these two time slices varies quite drastically, with nearly uniform globally cooler (ranging from −2.0 to −0.5°C) than PI temperatures simulated for LIG-130, whereas LIG-125 shows a more diverse response with areas of both distinct warming and cooling. Some similarity between the two simulations still exists, the areas of strongest warming in LIG-125 (the North Pacific Ocean, the Caribbean region of the Atlantic Ocean, the central region of the Arctic Ocean, the Sea of Okhotsk, and parts of the Amazon forest region in South America), are the same regions of LIG-130 that show slight warming relative to the PI simulation. Similarly, the regions of greatest cooling in LIG-125 (the Sahel and Sahara regions of Africa, the Indian subcontinent, the North Atlantic, as well as the equatorial Pacific and a small region southwest of Australia) are also regions of strongest cooling in LIG-130. Thus, although the magnitude of the temperature changes in these two simulations relative to PI is very different, the spatial distribution of the anomalous
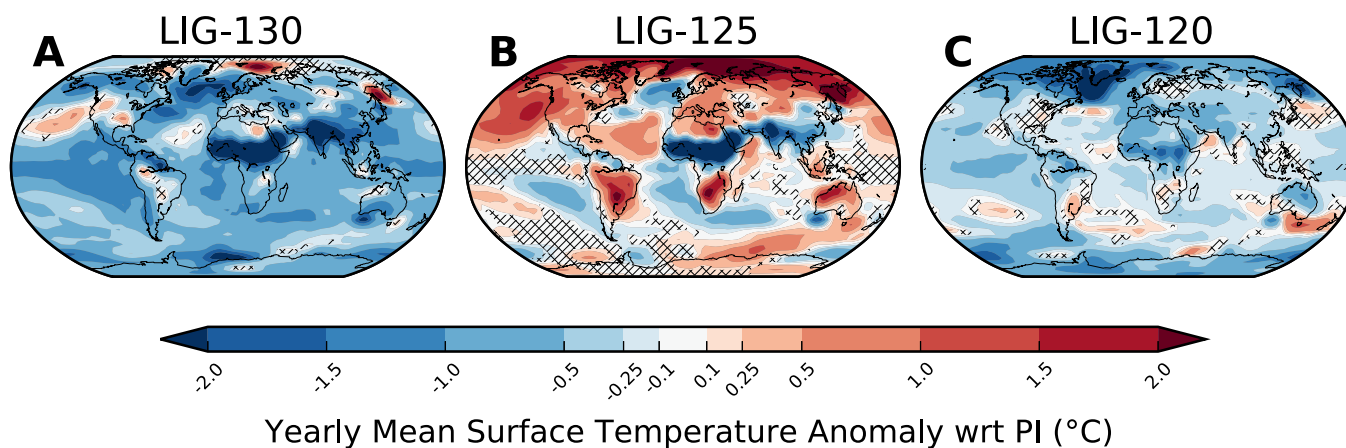
Figure 2. Changes in ST for the three simulated time slices ((a) LIG-130, (b) LIG-125, and (c) LIG-120) with respect to PI. Hatching overlays changes that are not significant based upon a 95% Student's *t* test.

responses is similar. This suggests that the simulated temperature changes can be mainly attributed to changes in incoming solar insolation.

If we further break down our analysis into seasonal changes (Figure 3), LIG-130 and LIG-125 are even more similar. Both simulations produce large-scale boreal summer warming over the Northern Hemisphere continents (anomalous temperature increases between 1.5 and 2.0°C), with slight cooling in the North Atlantic (between −0.5 and 1.0°C for LIG-130, and −0.25 and −0.5°C for LIG-125), and a stronger cooling over the Sahel region (–3.0 to −4.0°C) as well as over the Indian subcontinent. The winter responses of the two time slices also show similar distributions (strongest cooling over the Sahel region, Indian subcontinent, slight warming in the North Pacific, and strong warming in the central Arctic and Sea of Okhotsk), yet with different magnitudes.
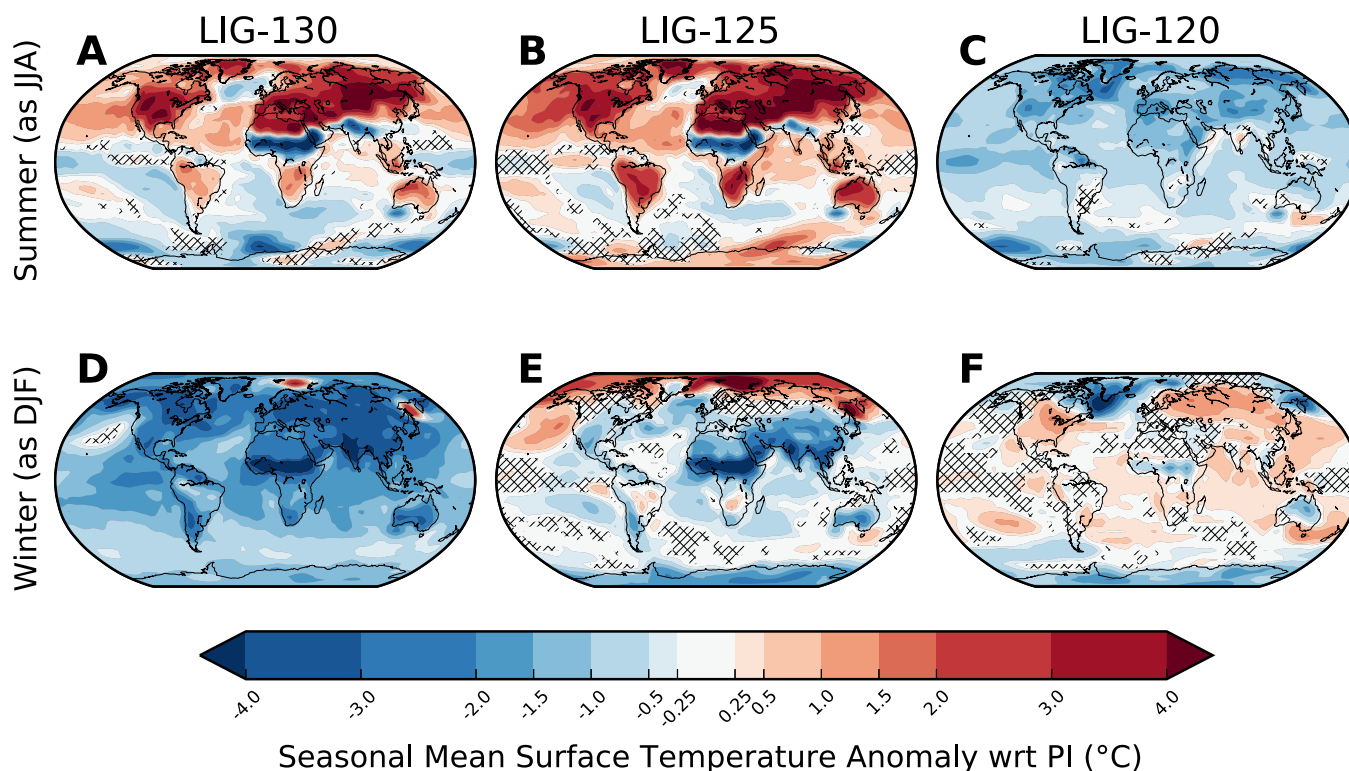

Figure 3. Seasonal changes in surface temperature as anomalies to PI, with boreal summer as the average for JJA, and boreal winter as DJF.

While the similarities in the distribution of the temperature responses, both seasonally and in the yearly means, might be connected to similar prescribed changes in solar insolation (shown in Figure 1, and broken down into individual orbital parameters in Table 1), the magnitudes of the simulated temperature changes between LIG-130 and LIG-125 are very different. Both internal feedbacks within the climate system and other prescribed boundary conditions could be responsible for these changes in simulated surface temperatures. In particular, the strong difference in the prescribed GHG forcing may be responsible for the difference in the magnitude of the responses. GHG values between the two simulations vary greatly. They are much lower in LIG-130 (relative to LIG-125: CO_2: −19 ppm, CH_4: −126 ppb, N_2O: −25 ppb), and as LIG-130 has GHG values that are considerably lower than for the PI, this change in insolation forcing can explain the simulated global cooling response.

Next, we examine the LIG-120 response in more detail. From the prescribed insolation forcing (Figure 1) and GHG concentrations (Table 1) we would expect a cooling of the yearly mean LIG-120 climate, as the GHG concentrations are lower relative to the PI simulation. Our GCM produces such temperature response, as shown in Figure 2c. Seasonally, prescribed insolation changes should result in a more heterogeneous temperature response. We simulate a globally cooler summer (between −0.25 and −1.0°C), which is a result of the slightly reduced GHG concentrations as well as a lagged response from a simulated cooler boreal spring, a season in which the prescribed insolation is strongly reduced relative to PI. Simulated winter temperature changes vary in space, too, with a pronounced high latitude cooling (−1.0 to −2.0°C) over the Arctic and the Greenland Ice Sheet. This may be a result of minimally changed insolation at high latitudes, as well as a sea-ice coverage that is very similar to that in the PI simulation (shown in the supporting information). An interesting land-sea contrast is simulated over Eastern Siberia and the West Bering Sea; however, a close examination of the insolation also shows here that incoming radiation values are slightly increased, with values of between +2.5 and 10 W/m^2 more energy than in PI. The temperature response to this small positive forcing anomaly may be further enhanced with a lag from the strong warming in late autumn.

If we compare our results to other paleoclimate simulation studies examining the LIG climate, we find that our model produces some interesting differences. One example would be the simulations performed by *Otto-Bliesner et al*. [2013], who used the CCSM3 model to generate time slices for the LIG. A striking difference between our realizations of both the LIG-125 and LIG-130 climates and theirs is a clear, seasonally persistent cooling signal in the North Atlantic in our study. *Otto-Bliesner et al*. [2013] instead report a simulated warming of +2–4°C (LIG-125), and +4–6°C (LIG-130) in this region. In *Lunt et al*. [2013], a multimodel ensemble assessment of the LIG is presented. Several models shown in this study, such as the Hadley Centre model (HadCM3) which has a comparable model resolution and complexity to our set up, also show a warming signal in the North Atlantic with a comparable temperature magnitude to that presented by *Otto-Bliesner et al*. [2013] for LIG-125. For LIG-130, HadCM3 shows only slight warming of between +1.0 and 2.0°C. However, the multimodel ensemble of all included models shows no significant change in this region. In a previous study by *Pfeiffer and Lohmann* [2016], who used the same model as applied in this study, a warming in the North Atlantic was also reported. However, this warming was caused by a modification of the Greenland Ice Sheet orography, and the study by *Pfeiffer and Lohmann* [2016] did not adapt the GHG values to the LIG level. The differences between our realizations of LIG climate states and those of the other groups mentioned above might stem from slightly different boundary conditions. For instance, *Otto-Bliesner et al*. [2013] utilized markedly higher concentrations of GHG (300 ppm CO_2 in LIG-130, relative to our value of 257 ppm CO_2). Furthermore, it has been well documented that different models react to climate forcings with various sensitives to a change in GHG concentrations; our model has a sensitivity of 4.1°C to a doubling of CO_2 concentrations (as stated, e.g., in *Haywood et al*. [2013]), compared to 2.7°C for CCSM3 and 3.2°C for HadCM3 [see *Otto-Bliesner et al*., 2013].

In a previous study with the GCM ECHOG model, which includes the atmospheric model ECHAM4, *Felis et al*. [2004] analyzed the simulated LIG temperature seasonality. They found an enhanced temperature seasonality in the Red Sea, in agreement with temperature reconstructions derived from fossilized corals. Our simulation with ECHAM5/MPIOM-wiso also indicates an enhanced seasonal amplitude in temperature; as shown in Figure 3: simulated boreal summer temperatures are warmer for LIG-130 and LIG-125, while boreal winter temperatures are slightly cooler. This is primarily a result of the increased seasonal amplitude of insolation, as shown in Figure 1.
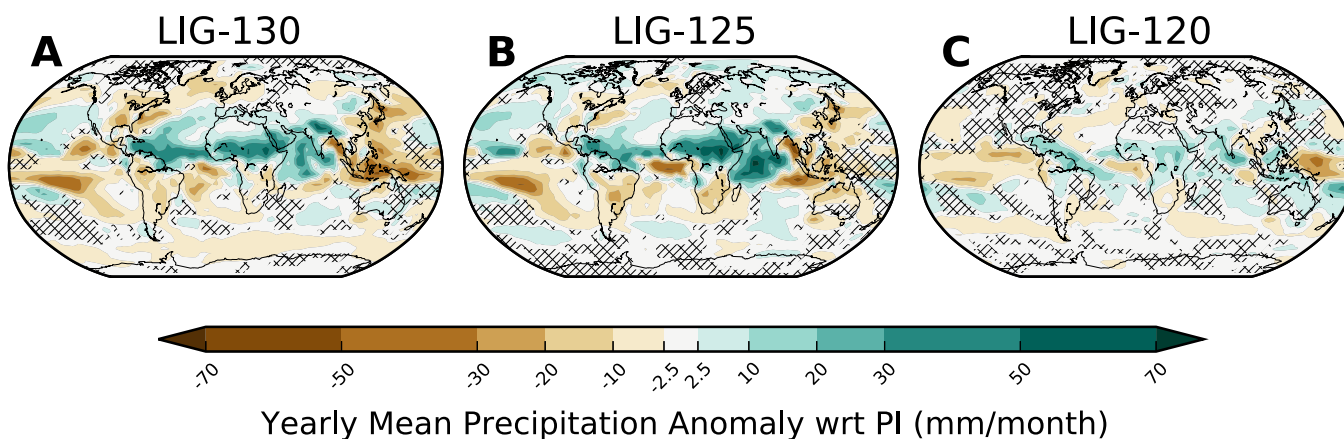
Yearly Mean Precipitation Anomaly wrt PI (mm/month)

Figure 4. As Figure 2, but showing yearly averaged total precipitation.

5.2. Changes in Physical Responses: Precipitation

Next, we analyze simulated changes of the hydrological cycle. LIG anomalies of the mean precipitation amount relative to the PI climate are shown in Figure 4. Contrary to the strong temperature differences between our simulations, the precipitation changes are more similar for LIG-130 and LIG-125, both in the climatology mean, and in the seasonal amplitude (Figure 5). For both LIG-130 and LIG-125, we simulate an increase in precipitation of between 20 and 50 mm/month over Saharan Africa as well as over the Indian subcontinent and the northern part of the Indian Ocean. The LIG-120 simulation, which was different from the other two LIG simulations with respect to the simulated surface temperature, shows similar changes in the precipitation amount and pattern, but the magnitudes of amount changes are reduced (10–20 mm/month, only).
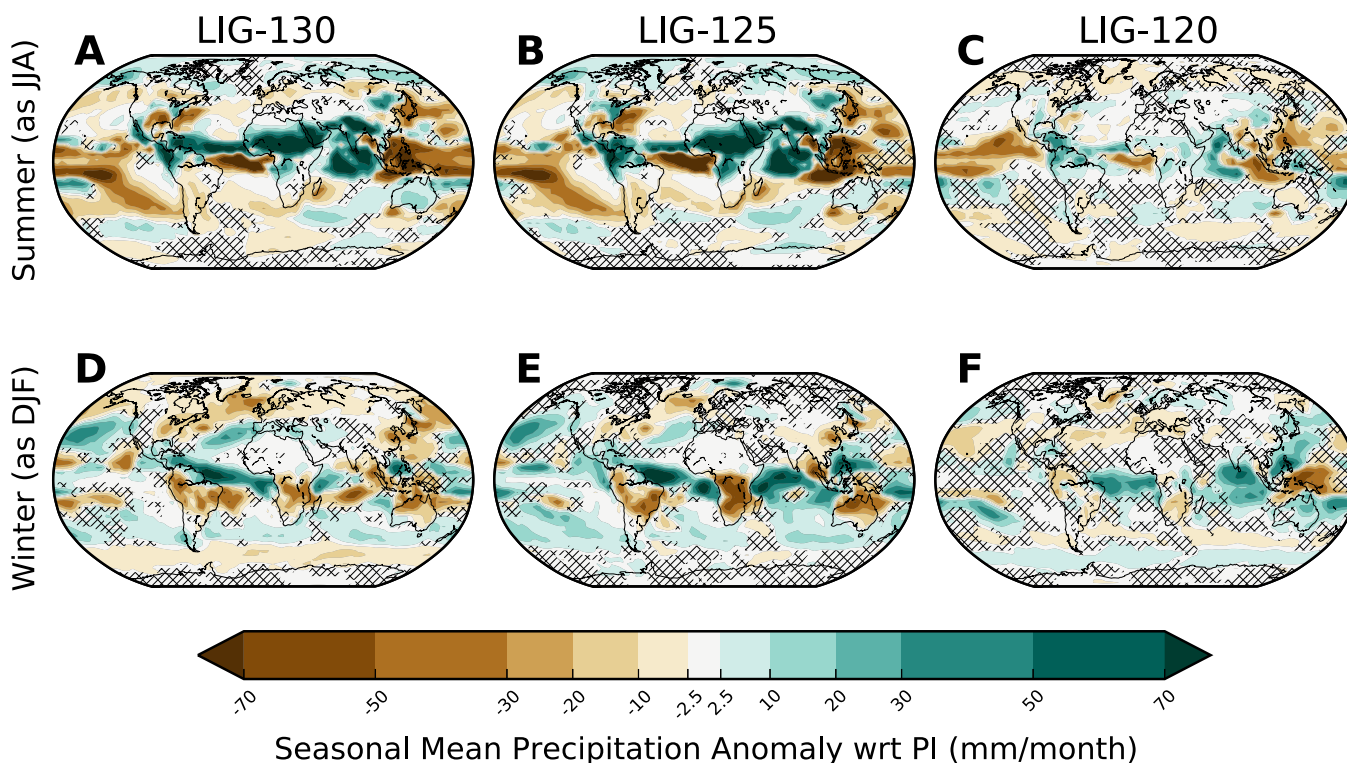

Seasonal Mean Precipitation Anomaly wrt PI (mm/month)

Figure 5. Anomalous summer and winter precipitation amounts relative to PI.

We can explain the changes seen in the global precipitation patterns as a result of the overall warmer climate of the LIG, which is especially reflected in the seasonal responses. Changes in the meridional temperature gradients cause a shift in the ITCZ, which can be seen in the dipole of the precipitation anomalies pattern over the Atlantic tropics during LIG-130 and LIG-125 summers. A resulting increase in cloud cover over the Sahara (not shown) also increases the albedo, causing a radiative feedback that leads to a cooling of the region (Figures 3a and 3b). Beyond the Atlantic realm, changes in the precipitation patterns could be attributed to an intensification of the hydrological cycle. Such increases in precipitation amount can be explained by fundamental physical mechanisms as a consequence of the Clausius-Clapeyron relation, as warmer air is able to hold more moisture [*Barron et al.*, 1989; *Trenberth et al.*, 2003]. This type of response in the hydrology for warmer-than-present day climates has been previously also reported for Pliocene climate simulations using the same GCM setup as in our study [*Stepanek and Lohmann*, 2012], and it is also seen in other modeling studies [*Haywood et al.*, 2013]. An invigoration of the hydrological cycle is also suggested to be a feature of warmer-than-present day future climate scenarios simulated in many IPCC projections [e.g., *Wild et al.*, 2008] (IPCC AR5, 2014).

5.3. Examination of the Isotopic Responses

Beyond the ability of a traditional GCM, the advantage of ECHAM5/MPIOM-wiso lies in the fact that it can simulate both physical as well as isotopic responses in Earth's hydrological cycle related to the prescribed past changes in orbital and GHG forcing. Figure 6 shows the yearly averaged anomalies in the isotopic composition of precipitation for the three simulated time slices during the LIG.

During both LIG-130 and LIG-125, we find a large-scale $\delta^{18}O$ depletion of down to $-2.5‰$ in precipitation over Saharan North Africa, as shown in Figure 6a. We furthermore find a $\delta^{18}O$ depletion with values between -0.5 and $-1.5‰$ over the Caribbean and North Atlantic, and this depletion signal extends over continental Europe and much of Asia. Over the equatorial Pacific, a slight $\delta^{18}O$ enrichment is simulated, with values between $+0.5‰$ and $+1.5‰$ above the PI values, and this signal extends over Australia and Indonesia. Over Greenland, a slight $\delta^{18}O$ enrichment of $+1.0‰$ in the north and a slight depletion of $-0.5‰$ in the southeast during LIG-130 can be detected, whereas during LIG-125, the isotopic signature over Greenland is more uniform, with relative enrichment ranging from $+0.5‰$ to $+1.5‰$.

In the LIG-120 experiment (Figure 6c), a $\delta^{18}O$ depletion over Greenland is found, with values $-1.0‰$ to $-1.5‰$ lower than in the PI simulation, a negative $\delta^{18}O$ anomaly not seen in the other LIG time slices. Over the Atlantic, precipitation is enriched in $\delta^{18}O$ rather than depleted during LIG-120, although this enrichment is only minor, with $\delta^{18}O$ values between $+0.0‰$ and $+0.5‰$ higher than the PI values. A slight $\delta^{18}O$ depletion in precipitation over Northern Africa is also simulated, yet it is not as strong as in the LIG-130 and LIG-125 simulations. The $\delta^{18}O$ enrichment simulated over the Pacific for the LIG-130 and LIG-125 period is also seen in this LIG-120 time slice simulation.

In Figure 7, the modeled $\delta^{18}O$ changes in precipitation for boreal summer and boreal winter are displayed. During both LIG-130 and LIG-125 summers, the isotopic composition of rainfall is depleted in $\delta^{18}O$ by
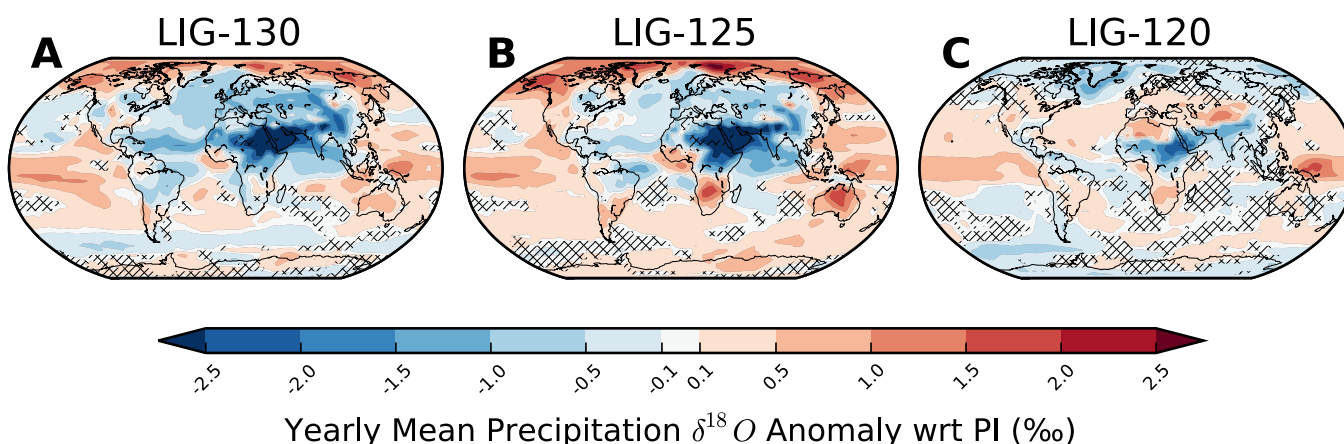

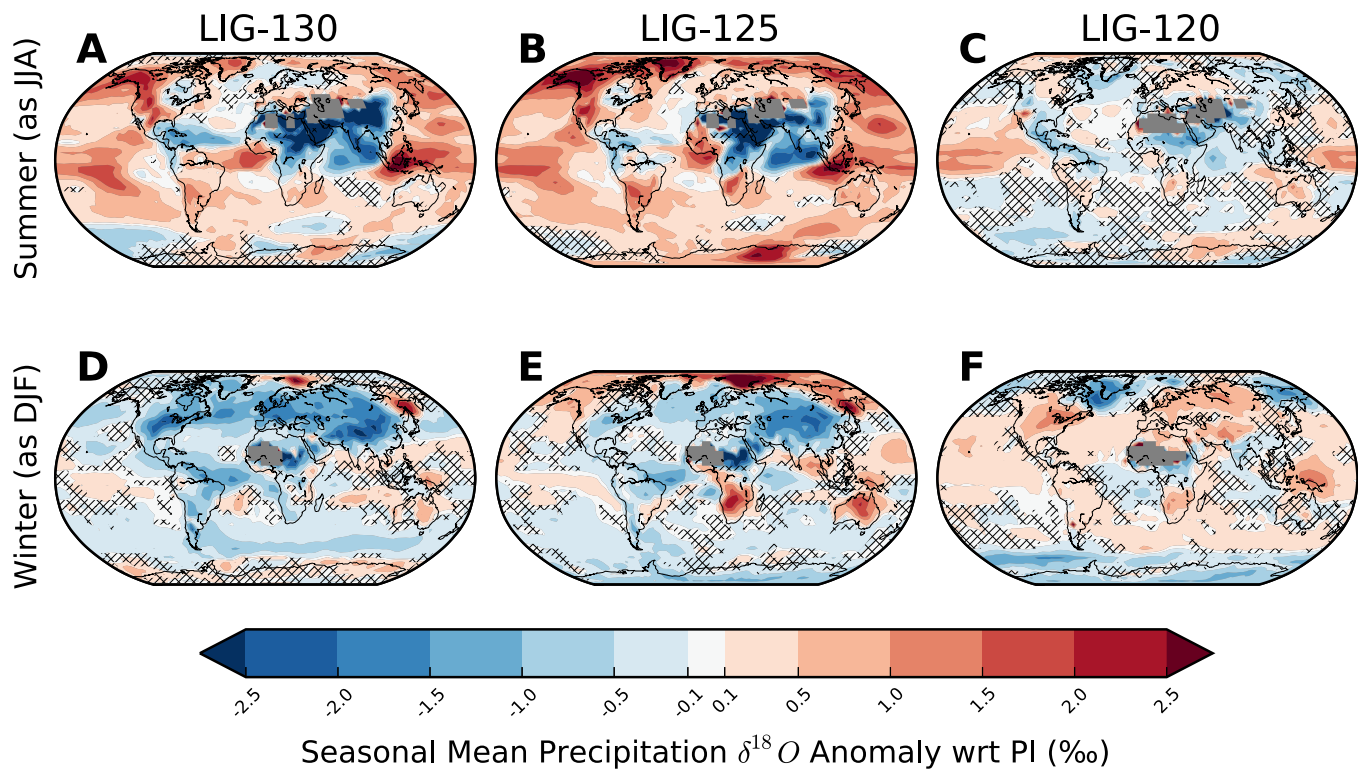**Figure 6.** As Figure 2, but showing yearly averaged $\delta^{18}O$ anomalies.

Figure 7. As Figure 4, showing δ^{18}O anomalies for summer and winter relative to PI.

between $-2.0‰$ and $-2.5‰$ over the Sahel region and Indian subcontinent and surrounding ocean. Additionally, precipitation over the tropical Atlantic is depleted in δ^{18}O by between $-0.5‰$ and $-1.5‰$. Apart from a slight area of depletion over the North Atlantic of less than $-0.05‰$, precipitation in the rest of the world is enriched in δ^{18}O by between $+0.5‰$ and more than $+2.5‰$.

During LIG-120 summers, the changes in the isotopic composition of precipitation are not as strong as for the other two time slices. However, there exists an exception over the Sahel region in Africa, where precipitation is depleted in δ^{18}O by $-0.1‰$ to $-0.5‰$, as well as over the equatorial Pacific, where δ^{18}O in precipitation is enriched by $+0.1‰$ to $+1.0‰$ as compared to the modeled PI values.

During LIG-130 and LIG-125 winter seasons, precipitation over most regions is depleted in δ^{18}O relative to the PI, with typical δ^{18}O anomalies of $-0.5‰$ to $-1.5‰$. Depletion is strongest over the continents, and relatively weaker depletion is taking place over the oceans. Some differences between the LIG-130 and LIG-125 simulations are seen over the Arctic, where LIG-125 winters reveal an enrichment of δ^{18}O in precipitation.

During LIG-120 winters, the precipitation δ^{18}O values are enriched by between $+0.1‰$ and $+0.5‰$ over the North Pacific, North and South Atlantic, European continent as well as over the Americas, as compared to the simulated PI values. Furthermore, a slight δ^{18}O depletion over the tropical Atlantic of $-0.5‰$ is simulated.

As isotope diagnostics has been implemented in all relevant model components of the fully coupled ECHAM5/MPIOM-wiso model, the model also simulates changes of the isotopic composition of different oceanic water masses. Changes for the surface ocean are shown in Figure 9 (and discussed below), as well as for a transect of the North Atlantic basin, shown in the supporting information.

After this description of the simulated changes of δ^{18}O in precipitation during the various phases of the LIG, we now analyze different processes, which might cause these different distributions of δ^{18}O in precipitation. We divide this part of the discussion into several parts, describing first isotopic changes that can be primarily explained by changes in net precipitation, and second isotopic changes that can be primarily explained

by changes in temperature. Comparison to other isotopically enabled simulations of the LIG [e.g., *Herold and Lohmann*, 2009; *Sjolte and Hoffmann*, 2014; *Holloway et al.*, 2016] is also provided in order to place our simulations into context with other studies.

5.4. Isotopic Signals Caused by Changes in Precipitation

For all our LIG simulations, a strong depletion is simulated in δ^{18}O in precipitation over the Sahara region. This may be attributed to the so-called amount effect (an inverse relationship between δ^{18}O in precipitation and the amount of precipitation, itself; e.g., explained in *Aggarwal et al.* [2016]), since the overall amount of precipitation increases in this region in all three LIG simulations. The dominance of the amount effect is also seen over the equatorial Pacific as well as over southern Africa; here, overall less rainfall, and correspondingly, an enrichment of δ^{18}O, is simulated. Further examples of the influence of the amount effect on the δ^{18}O values of Indian and Pacific tropical precipitation are shown in the supporting information.

Next, we analyze the connection between seasonal changes in precipitation and related seasonal changes in the isotopic composition of precipitation. During LIG-130 and LIG-125, a particularly strong increase in precipitation over the equatorial latitudes is simulated during the summer season. For the same equatorial band over the Atlantic, Saharan Africa, and the Indian subcontinent, a strong LIG depletion of δ^{18}O in summer precipitation is modeled. Just south of this region of increased rainfall, we detect a simulated drying, which is mirrored by an enrichment of δ^{18}O in summer precipitation. For LIG-120, the same relationship between precipitation amount and δ^{18}O in precipitation is seen over this region. However, the magnitude of precipitation increase is much smaller in the LIG-120 simulation as compared to the LIG-130 and LIG-125 experiments. In boreal winters, the model simulates an increase in precipitation just south of the equator for the LIG-130 and LIG-125 climate, with a corresponding depletion in the δ^{18}O signal of precipitation. During LIG-120 boreal winters, the simulated changes in precipitation and in the isotopic signature of precipitation are not as strong as for the other two time slices, yet here also some areas of increased precipitation and a corresponding depletion in the δ^{18}O signature of precipitation can be detected (in particular over the South Atlantic and Indian Ocean).

Several previous studies using atmosphere-only models equipped with stable water isotope diagnostics have already investigated changes of the Earth's hydrological cycle during the LIG. *Herold and Lohmann* [2009] discuss simulated changes in the isotopic composition of precipitation using the isotope-enabled version of ECHAM4. They also argue that major LIG changes in δ^{18}O in precipitation can be explained by the amount and continental effects, as their LIG climate simulation demonstrates a relative increase in total precipitation over North Africa relative to the PI simulation, similar to the results we have shown in Figures 5 and 7. Additionally, they find a shift in the isotopic west-east gradient, with more depleted Eemian isotope values towards the east compared to present day, as a result of an intensified zonal transport of moisture from the Atlantic.

While this is not the focus of this manuscript, the results presented in our study (depletion of $\sim +1.0$ to $+1.5\permil$ in the African subtropics relative to PI in LIG-125, Figure 7b) confirm that these previous findings hold true for this newer, fully coupled version of ECHAM5/MPIOM-wiso, suggesting that while not all effects can be account for in an atmosphere-only model, such simulations still provide reasonable, first-order results.

Sjolte and Hoffmann [2014] also used the atmosphere-only model ECHAM4 to study changes of the tropical hydrological cycle during the LIG. Similar to the study of *Herold and Lohmann* [2009] as well as our own results, they found that LIG changes of δ^{18}O in tropical precipitation are caused by a variety of above mentioned factors. Interestingly, their anomalous SSTs are quite different in the Pacific Ocean as compared to *Herold and Lohmann* [2009] and our results presented here, indicating an inherent climate mode in the Atlantic-Indian Ocean realm.

Such atmosphere-only simulations are useful stepping stones in the model development process toward a fully coupled isotope-enabled GCM. It is critical to mention here that while atmosphere-only paleoclimate simulations with stable water isotopes may provide an important first impression of the isotopic signal distribution of a particular time period, some important feedbacks may not be accounted for without fully coupling to an ocean model. Primarily, changes in the isotopic signature of the source region would not be accounted for (as shown in Figure 9), which would necessitate an isotope-enabled ocean model. As an

example, in our scenarios particularly strong changes in the surface ocean are simulated in North Atlantic (–0.4 to −0.6‰ in LIG-130 and LIG-125 relative to PI), as well as in the Indian Ocean (–0.2‰ to −0.4‰ for LIG-130 and LIG-125). Additionally, dynamic vegetation has an important impact, and changes of temperature and soil wetness can be responsible for δ^{18}O changes of up to 4‰, as shown by *Haese et al.* [2013].

5.5. Isotopic Signals Linked to Changes in Surface Temperature

While we can explain changes in the isotopic signature of rainfall in the equatorial and tropic latitudes by related changes in the amount of precipitation, simulated δ^{18}O changes in midlatitudinal to high-latitudinal regions appear to be stronger linked to changes in the surface temperature, as already described by *Dansgaard* [1964] and *Rozanski et al.* [1992]. For example, the North Atlantic significantly cools between −0.5 and −1.5°C in our LIG-130 and LIG-125 simulations. In the same region, we detect a slight depletion of δ^{18}O in precipitation. Another example can be found in the LIG-120 simulation, where an annual mean cooling over the Arctic Ocean and the Greenland Ice Sheet, as well as over the Antarctic Ice Sheet (Figure 2c), and correspondingly, a slight depletion of δ^{18}O in precipitation (Figure 6c) can be detected.

In some regions, a strong seasonality appears to mask a clear link between annual mean surface temperature and δ^{18}O changes. For example, over the most northern regions of North America, Greenland, and Siberia, the annual mean LIG changes of surface temperature and isotopic composition of precipitation do not seem to be related. This is especially true during LIG-130, where a cooling is simulated over these northern regions, yet the isotopic composition of rainfall is still enriched in δ^{18}O. However, for both summer and winter season in the LIG-130 and LIG-125 climate, regions with a seasonal warming (cooling) also show a seasonal enrichment (depletion) of δ^{18}O in precipitation. For the LIG-120 simulation, we can also find some seasonal dependencies of the modeled surface temperature and δ^{18}O changes. For example, the LIG precipitation over North America becomes slightly enriched in δ^{18}O, even though a slight cooling is simulated in the annual mean temperature change. However, if the summer and winter temperature and δ^{18}O changes are examined, both quantities show a corresponding response.

5.6. Comparing to Paleoclimate Reconstructions

It is important to examine to what extent the simulated isotopic changes in ECHAM5/MPIOM-wiso are comparable to measured isotopic values from paleoclimate archives to give some sense of the model's ability to accurately reproduce the real-world climate of the LIG. To do so, we compare the simulated results of δ^{18}O in precipitation to ice core measurements of six different Antarctic ice cores, which have been compiled in *Masson-Delmotte et al.* [2010], as well as the NEEM ice core recently drilled from Greenland [*NEEM Community Members*, 2013]. In addition, we compare our model results against the δ^{18}O variations in calcite ($\delta^{18}O_c$) measured in several speleothem records, from caves located in China, France, Italy, and the Middle East. For all selected speleothem records, both PI and LIG values have been published (see the supporting information for details). For our model results, the isotopic signature of speleothem calcite is calculated from the simulated annual mean precipitation-weighted δ^{18}O value and the annual mean surface air temperature at each cave location, as it has been done in *Werner et al.* [2016] (this method is expanded upon in the supporting information). The results of this comparison are shown in Figure 8.

The speleothem comparison displays a good agreement between the model values and the δ^{18}O measurements. Except from the measurements from the Chinese caves during the early LIG, simulations and measurements yield qualitatively (same sign of anomalous δ^{18}O change relative to PI) comparable LIG $\delta^{18}O_c$ anomalies relative to the PI climate. The mismatch in the Chinese caves could be attributed to a number of model deficiencies that might play a role in this region. First, the model grid is coarse, thus possibly masking finer scale features; the enrichment seen in the western Pacific possibly could extend into the speleothem locations and is simply eliminated by the resolution. Furthermore, the model orography is smoothed due to the coarse lateral resolution, and any elevation effects (such as enrichment higher up an orographic gradient due to previous rain-out) would also be incorrectly represented.

Examining the model-data differences at the ice core locations, we find that in particular during LIG-130 the model underestimates the amount of δ^{18}O enrichment seen in the Antarctic ice cores, suggesting that the simulated LIG-130 climate in Antarctica is too cool, a difficulty also seen in other isotope-enabled simulations [e.g., *Holloway et al.*, 2016]. This deficit might be related to the negligence of potential changes in the Antarctic Ice sheet's geometry during the LIG in our model setup or in changes to the sea-ice cover. It has
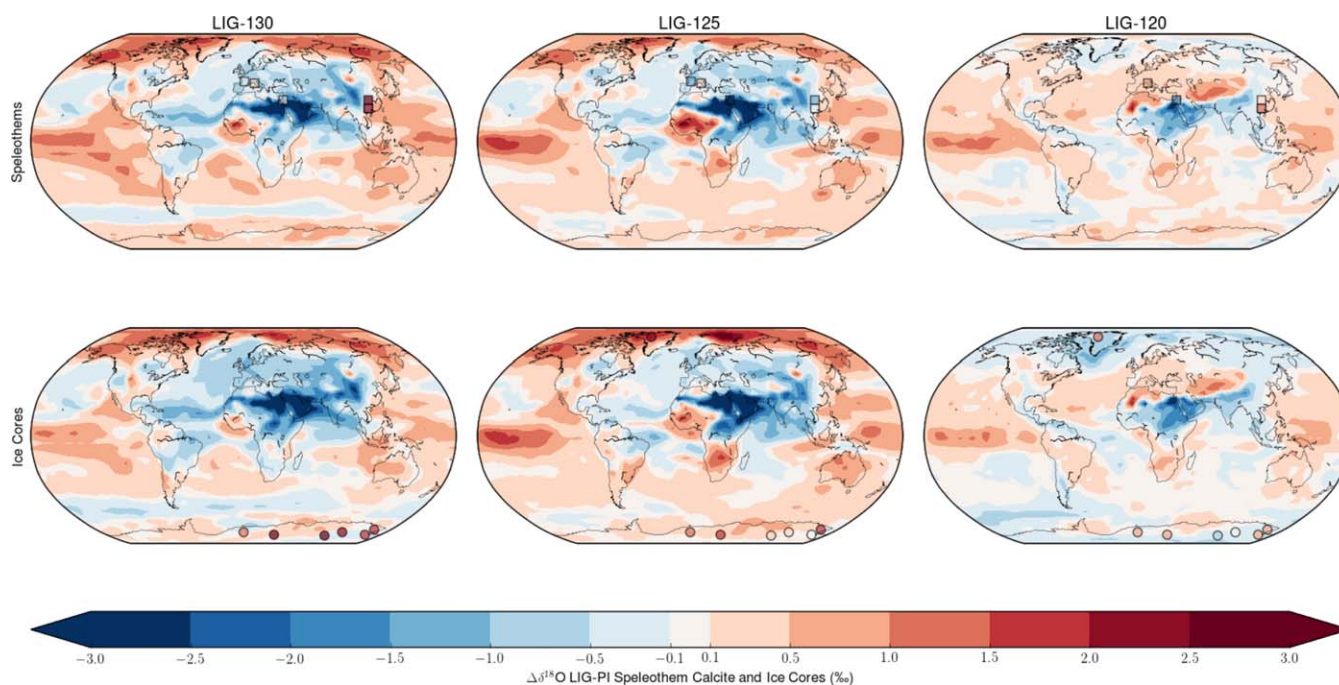
Figure 8. Comparison of six Antarctic ice cores (circles), one Greenland ice core (circles), and several speleothem records (squares) to isotopic values simulated by ECHAM5/MPIOM-wiso. In order to compensate for potential age uncertainties, each comparison is made against a 1000 year average for the paleoclimate record (for LIG-130, ages from 130.5 to 129.5 ka B.P. were chosen in the ice core, etc.).

been demonstrated that the West Antarctic Ice sheet may have disintegrated during the Last Interglacial [*Sutter et al.*, 2016], and sea level reconstructions indicate LIG changes of +6 to +9 m above the PI sea level, indicating that some ice from the Antarctic Ice Sheet must have been melted during this time [*Kopp et al.*, 2009; *Dutton et al.*, 2015]. *Sutter et al.* [2016] also found that an ocean warming of +2 to +3°C (relative to PI) is required to trigger a partial melting of the West Antarctic Ice Sheet. In our LIG-130 simulation, the Southern Oceans do not warm significantly, and this underestimation of marine temperature change may be responsible for the mismatch between the simulated $\delta^{18}O$ values and the ice core data. For the LIG-125 climate, simulated $\delta^{18}O$ changes and Antarctic ice core data agree quite well. For the LIG-120 simulation, we find a similar result as for LIG-130: Modeled $\delta^{18}O$ values in precipitation over the Antarctic ice sheet are again too depleted, suggesting an underestimation of the warming of Antarctica during the late LIG.

We furthermore compare our model results against the NEEM ice core data, and find that for the LIG-125 time period, simulated and ice core $\delta^{18}O$ values match in the sign of the change, with an enrichment of +2.1‰ in the ice core record and +1.3‰ in the simulation. The magnitude of $\delta^{18}O$ change may be underestimated in the LIG-125 simulation as no change of Greenland's ice sheet height has been considered in our model setup. Sea level reconstructions indicate that the Greenland Ice Sheet was likely reduced during the LIG [*Dutton et al.*, 2015]. For the LIG-120 climate (modeled −0.7‰ and measured +1.0‰), $\delta^{18}O$ changes do not agree in their sign. Again, it is likely that the simulated LIG-120 climate is too cold and underestimates a potential warming of this region.

5.7. Sensitivity Tests: Atmosphere-Only Simulations and a Warming of the Southern Ocean
So far, several studies using atmosphere-only simulations have been performed in order to examine LIG changes of $\delta^{18}O$ in precipitation and its relationship to temperature changes [e.g., *Masson-Delmotte et al.*, 2011; *Sime et al.*, 2013] on a local and regional scale.

For an extended comparison of our model results with these previous studies, we have performed three additional simulations (LIG-130-A, LIG-125-A, and LIG-120-A) with the atmosphere-only model ECHAM5-wiso. The required prescribed ocean boundary conditions have been derived from calculated multiyear monthly mean of 100 years for SST and sea-ice concentration from the fully coupled simulation. The isotopic composition of surface ocean water (Figure 9) has also been derived from the fully coupled simulation.
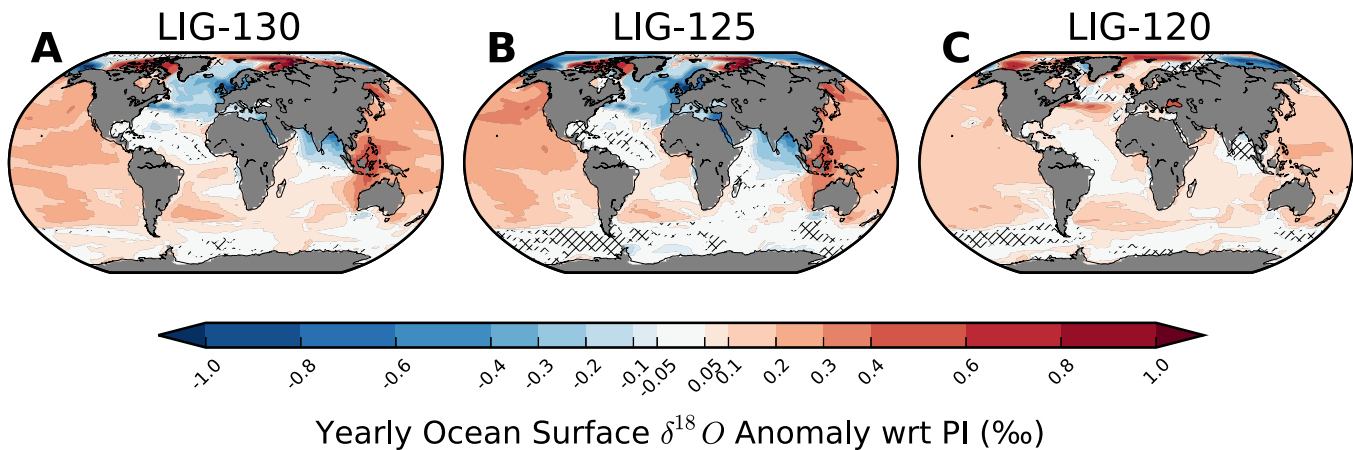
Figure 9. Comparison of LIG-130, LIG-125, and LIG-120 surface water δ^{18}O relative to PI, as shown for precipitation in Figure 6.

Furthermore, we have applied the same boundary conditions for the solar insolation and greenhouse gas concentrations as for the fully coupled LIG simulations, and initialize from a modern-day, nondynamic vegetation. The differences between the atmosphere-only simulations versus the fully coupled simulations are quite small, in general (they are shown exemplarily for the LIG-130 simulations in the supporting information). With the exception of the Saharan desert, we detect only slight differences in the simulated pattern of δ^{18}O$_P$ changes. This agreement suggests that atmosphere-only modeling approaches can provide a useful tool for studying δ^{18}O changes in precipitation during the LIG. However, a fully coupled model setup, including a dynamical vegetation scheme, will be required for the study of past isotopic changes in marine and terrestrial archives.

Next, we apply our atmosphere-only model setup for testing the influence of warmer oceanic boundary conditions on δ^{18}O changes in precipitation over Antarctica during the LIG-130 climate. All boundary conditions are the same as in the standard atmosphere-only simulation (LIG-130-A), with sea-ice coverage, sea surface temperature, and ocean surface δ^{18}O values extracted from the fully coupled LIG-130 simulation. However, we warm the Southern Ocean (SO) immediately around the Antarctic continent by +2°C, linearly decreasing the warming down to 0°C at 50°S. Sea-ice coverage is adapted to these temperature changes by partial melting. The modeled δ^{18}O values in precipitation of this LIG-130-A simulation with a warmed ocean, along with a comparison of modeled δ^{18}O changes and related Antarctic ice core data, are shown in Figure 10, and a table is shown in the supporting information. The warmer SO generates more enriched values over the Antarctic continent, rectifying the mismatch during LIG-130 between the simulated values and the measured ice cores.
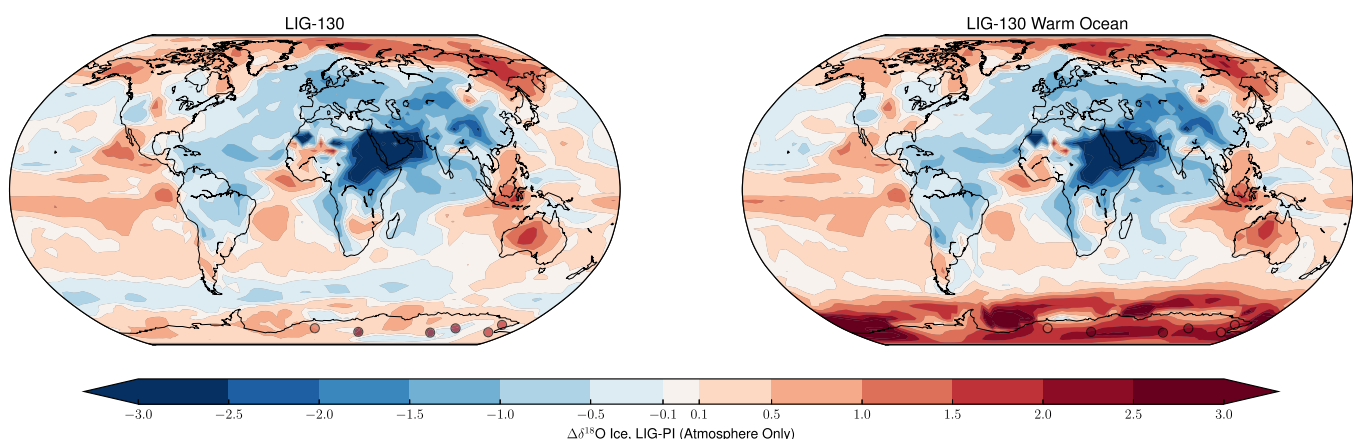

Figure 10. Results of a sensitivity test, warming the Southern Ocean by 2°C. The model-data mismatch between the ice core measurements and the simulation reduces considerably.
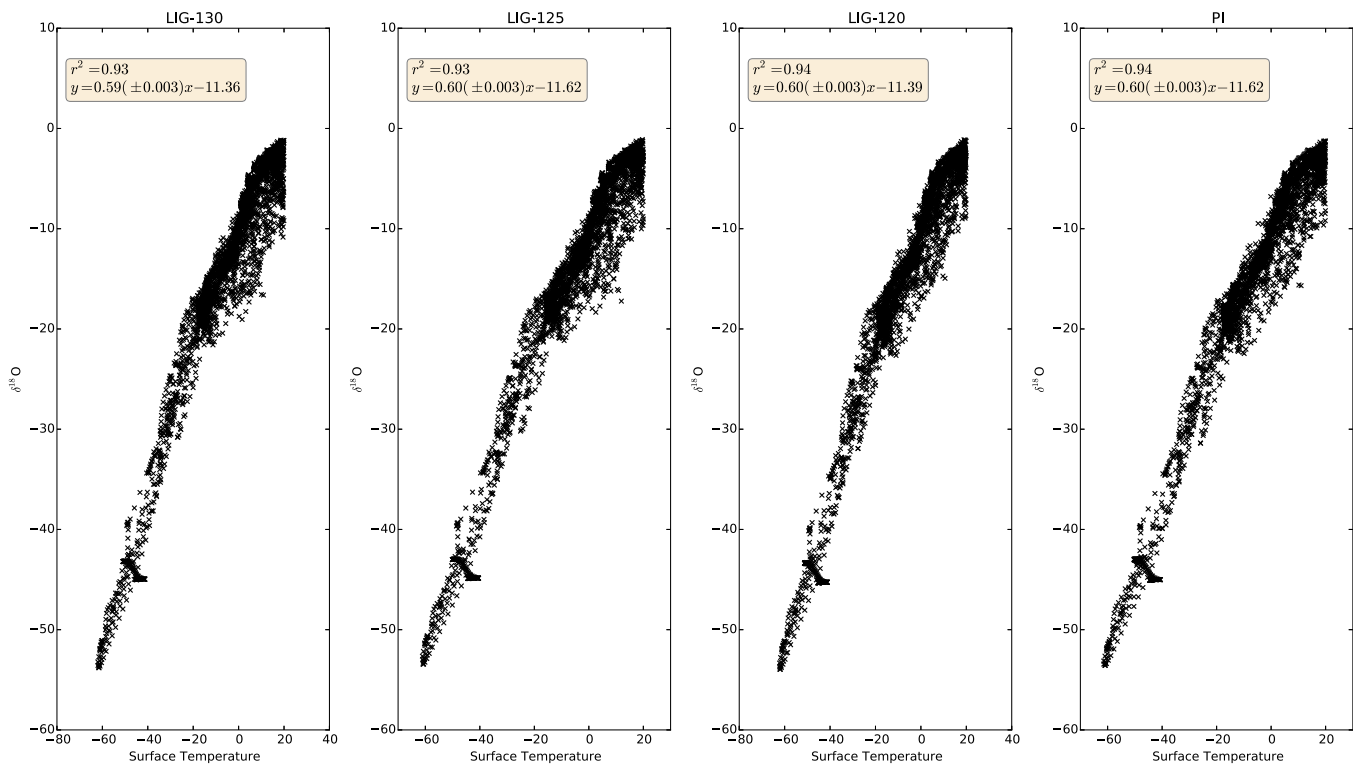
Figure 11. Scatterplots showing the relationship between $\delta^{18}O$ and temperature over all model grid points where the average mean annual is less than 20°C. The equation of the regression line is given in the legend for each simulation.

5.8. Stability of the δ^{18}O/T Relationship

Finally, we examine the relationship between simulated $\delta^{18}O$ and temperature changes, as this relationship allows the application of stable water isotope data for reconstructing past temperatures. First, we evaluate if our model can reproduce the modern spatial relation between annual mean temperatures and $\delta^{18}O$ in precipitation on a global scale, and analyze if the slope of the regression line between $\delta^{18}O$ and T remains stable throughout the LIG. For this analysis, we select only grid points with a mean annual temperature below 20°C to ensure that only locations with a dominant temperature dependency are included in the calculations.

For the control simulation of the preindustrial climate, we find a spatial $\delta^{18}O$-T regression slope of $0.60 \pm 0.003\%_0/$°C, whereas we find a slope of $0.59 \pm 0.003\%_0/$°C, $0.60 \pm 0.003\%_0/$°C, and $0.60 \pm 0.003\%_0/$°C for the simulations of LIG-130, LIG-125, and LIG-120, respectively (Figure 11). We conclude that the spatial relationship between temperature and $\delta^{18}O$ in precipitation does not change significantly on a global scale between the simulated different climatological mean states of the LIG and PI period.

For the PI climate, the simulated spatial $\delta^{18}O$-T slope is approximately 0.1‰/°C lower than the observed value of 0.69‰/°C [*Dansgaard*, 1964]. This finding is in agreement with the results reported in *Werner et al.* [2016]. In is also in agreement findings from several atmosphere-only isotope models (e.g., CAM2 [*Lee et al.*, 2007], LMDZ4 [*Risi et al.*, 2010], and ECHAM5-wiso [*Werner et al.*, 2011]), which often simulate a spatial gradient that is smaller than the observed one. *Werner et al.* [2011] have demonstrated that improving the model's spatial resolution can partially rectify this model bias. However, increasing the model resolution comes with higher computational costs and is often not possible for paleoclimate simulations that require a long integration time.

Next, we analyze the temporal relationship between temperatures and $\delta^{18}O$ in precipitation changes and then compare the simulated spatial and temporal $\delta^{18}O$-T slopes. For every LIG time slice simulation, the temporal gradient m of every grid box is calculated as $m = (\delta^{18}O_{LIG} - \delta^{18}O_{PI})/(T_{LIG} - T_{PI})$. We restrict our calculations to those grid cells where the following conditions are met: (1) simulated mean annual temperature of the grid cell is lower than 20°C for both PI and LIG climate. (2) The model simulates a significant
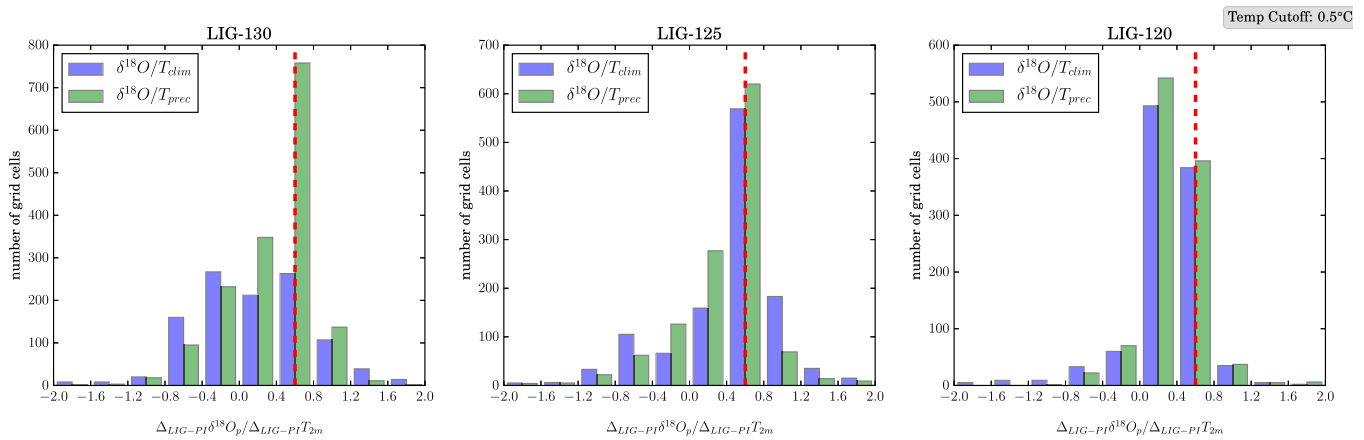
Figure 12. Histogram of the change in the δ^{18}O/T relationship for all grid points where the following three conditions are met: (i) average mean annual temperature is lower than 20°C. (ii) Absolute change in temperature between the LIG time slice and the PI control simulation is at least 0.5°C. (iii) The change in both temperature and isotopic composition is significant based upon a 95% confidence interval. Blue bars indicate the number of grid cells for each δ^{18}O/T quotient for climatology mean temperatures, whereas green bars indicate the number of grid cells where we utilize precipitation-weighted temperatures rather than climatologically averaged ones.

change in both mean annual δ^{18}O as well as mean annual temperature between the PI and the LIG climate, with significance determined by a *t* test considering a 95% significance interval, and a sample size N of 100 simulation years for both δ^{18}O and surface temperature. (3) Absolute temperature difference between the examined LIG time slice and the PI simulation is equal or above a threshold value of 0.5°C. These three criteria are applied to ensure that only locations with a dominant temperature dependency and with simulated LIG temperature and δ^{18}O changes well above the simulated interannual variability are included in the calculations.

We present the simulated temporal δ^{18}O-T slope of all selected grid cells as a frequency distribution in Figure 12 (blue portions of the histogram), and the corresponding global maps are shown in Figure 13. Upon initial examination, it appears as if the δ^{18}O-T relationship is not only varying for the different LIG time
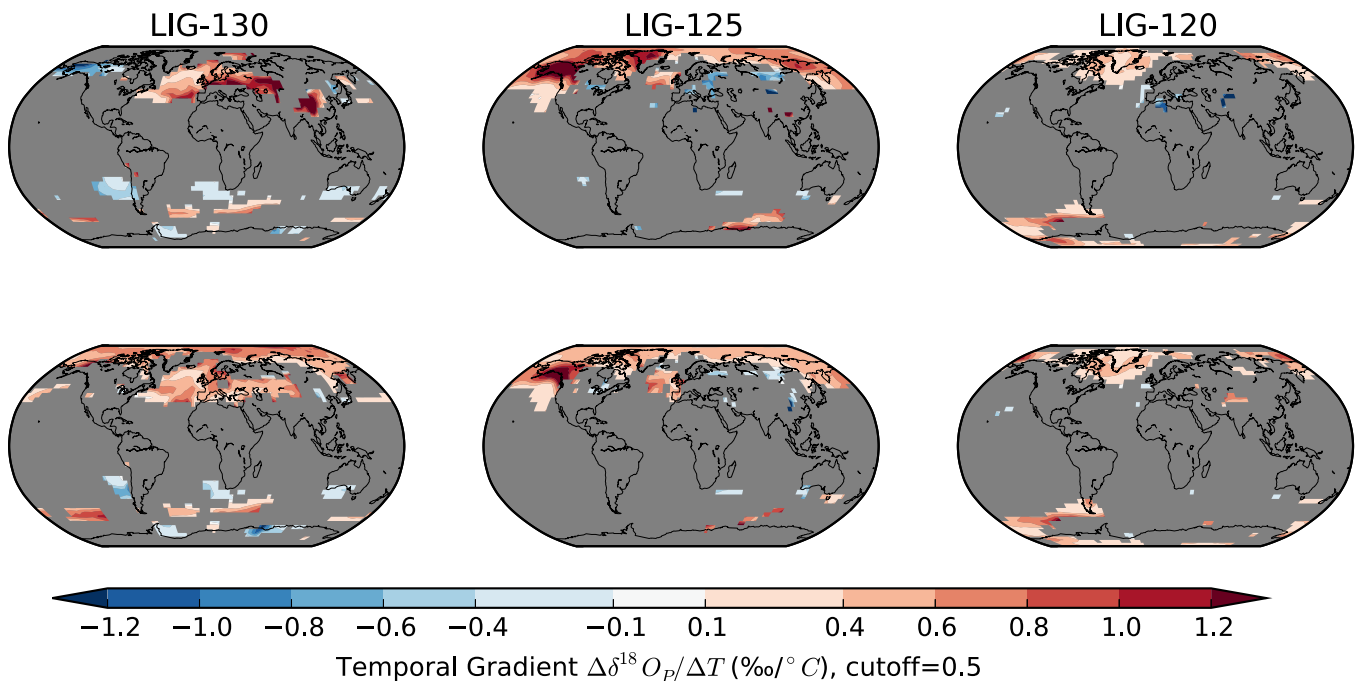

Figure 13. Spatial distribution of the Δ^{18}O/ΔT quotient. (top) The quotient with climatology averaged temperature changes and (bottom) the quotient with precipitation-weighted averages.

periods but also can have a negative slope at certain locations. Thus, our results might indicate either a "selection" or a "recorder" problem.

A "selection" problem might exist if we have included grid cells in our analyses, where simulated $\delta^{18}O$ and temperature changes are not linked, but controlled by other factors (e.g., changes in precipitation amount, source regions, and/or water transport pathways). In this case, the calculation of a temporal $\delta^{18}O$-T slope is meaningless and can easily result in negative values. The "selection" problem can be decreased by choosing a higher LIG temperature change threshold in our analyses.

A "recorder" problem might exist in some grid cells, where the annual mean value of $\delta^{18}O$ is biased by a strong change of seasonality (or intermittency) of the precipitation amount [e.g., *Steig et al.*, 1994; *Sime et al.*, 2009] or other effects like soil properties [*Lohmann et al.*, 2013b]. To identify grid cells affected by the "recorder" problem, we determine precipitation-weighted annual mean temperature anomalies of the different LIG simulations and recalculate the temporal $\delta^{18}O$-T slopes of all grid cells, using precipitation-weighted instead of arithmetic mean annual temperatures. Precipitation weighting is done by using both monthly temperatures as well as precipitation amounts of 100 simulation years to calculate the long-time mean annual precipitation-weighted temperature T_p.

For the "recorder" problem, we find that the frequency distribution of the temporal LIG $\delta^{18}O$-T gradients shift closer to the value of modern spatial $\delta^{18}O$-T-relationship, if precipitation-weighted temperatures are considered (shown in the green portions of the histogram in Figure 12). Despite this shift, a relatively large portion of the grid cells still reveals a negative $\delta^{18}O$-T slope. However, if we increase our temperature cutoff to 1.5°C (supporting information Figures S5 and S6) most grid boxes with negative $\delta^{18}O$-T slopes are removed from our analyses.

Our findings suggest that great care must be taken when reconstructing LIG temperature changes from measured or modeled $\delta^{18}O$ anomalies, as the spatial and temporal gradients do not always match. A "recorder" problem, related to a pronounced seasonality of precipitation in many regions, might substantially alter the temporal $\delta^{18}O$-T relationship for the LIG. Furthermore, our simulation results suggest that the assumption of a positive temporal $\delta^{18}O$-T relationship appears to only be valid if the magnitude of absolute LIG temperature changes is rather large (beyond 1.5–2°C). For areas with a lower temperature change during the LIG, the conversion of $\delta^{18}O$ changes into temperature changes might lead to inaccurate results.

These considerations might not be specific to the LIG. For a study of the Last Glacial Maximum (LGM) with the same fully coupled model setup, *Werner et al.* [2016] also reported potential biases of the classical $\delta^{18}O$ paleothermometer approach. However, since the magnitude of the temperature changes between LGM and PI climate is generally large, far fewer grid cells with negative $\delta^{18}O$-T slopes were found in this case.

For Antarctica, we find a temporal slope of 0.09‰/°C averaged over all of the ice core locations for the LIG-130 coupled simulation (range from a minimum of −0.22 to +0.59; table of slopes shown in the supporting information). This temporal slope is substantially different from the observed modern spatial gradient of 0.8‰/°C [*Masson-Delmotte et al.*, 2008]. However, for our simulation including a warm Southern Ocean, which shows a better agreement between simulated LIG $\delta^{18}O$ changes and ice core data, the average temporal slope is +0.69‰/°C, much closer to the modern spatial one. These results demonstrate that a good model-data match of past $\delta^{18}O$ changes is a crucial prerequisite for determining temperature-isotope relations with the help of isotope-enabled climate models.

Our results are also in line with the findings of previous studies with atmosphere-only models, which have focused on a model-data comparison for $\delta^{18}O$ signals in polar precipitation under present and warmer climate conditions. Several simulations with the isotope-enhanced model versions of LMDZ, HadCM3, and ECHAM4 under varying interglacial and future warming boundary conditions revealed inconsistent temporal and spatial $\delta^{18}O$-T slopes for both Greenland [*Masson-Delmotte et al.*, 2011; *Sjolte et al.*, 2011; *Sime et al.*, 2013] and Antarctica [*Sime et al.*, 2008]. Potential past changes in the seasonality of precipitation were also identified as highly important in these studies, especially for Greenland. A further study with the fully coupled isotope-enabled GCM HadCM3 [*Tindall and Haywood*, 2015], which is comparable to our coupled model setup, also concluded that the $\delta^{18}O$-T relationship might have changed in time and space. However, this simulation was performed for the warm climate of the Pliocene, not the LIG.

6. Conclusions, Limitations, and Outlook

In this study, we examined three climate states during the LIG, for 130, 125, and 120 kyr before present using a fully coupled general circulation model enhanced with stable water isotopes, provide a model validation against two paleoclimate archives, and examine the utility of the δ^{18}O/T temporal relationship for reconstructing past temperature changes. We found strong seasonal dependencies in the responses of δ^{18}O in precipitation. While we determined that the relationship between δ^{18}O and temperature remains stable throughout the LIG based upon a globally averaged spatial relationship, when attempting to use this spatial relationship to recreate temperature anomalies, we find that the δ^{18}O/T temporal quotient has a large degree of heterogeneity and deviates from the spatial relationship. If we filter our results and examine strong temperature changes only, the amount of variation in the δ^{18}O/T quotient decreases, and the quotient values approach the value of the spatial δ^{18}O/T relationship. Yet there are still areas with inconsistent slopes. Such inconsistency indicates a "recorder problem" in δ^{18}O in these areas and suggests that the classic paleothermometer approach may not be appropriate to understand smaller temperature changes in some regions during the LIG.

There are several potential improvements that we should consider for future studies of the LIG. Primarily, we did not modify the continental ice sheet geometry or extent during our simulations, although there have been suggestions [e.g., *Pfeiffer and Lohmann*, 2016, and references therein] that the LIG Greenland Ice Sheet may have been smaller than at present. Our justification for prescribing an identical PI ice sheet in all LIG simulations was to minimize a possible uncertainty in our climate forcing. While ice sheet geometry and extent both have an important role in climate feedbacks, examining the effect of ice sheet geometry on isotopic response is beyond the scope of this study.

Furthermore, the primary advantage of this new modeling approach has not yet been fully leveraged. By enabling our climate model to simulate stable water isotopes, we can produce more direct comparisons between geochemical climate proxies and climate simulations, and allusions to such comparison studies have already been made in several LIG proxy studies, such as *Capron et al.* [2014]. Such combined isotope studies will allow us to potentially uncover climate mechanisms that may have previously been difficult or impossible to analyze due to the inherent challenge in comparing geochemical proxy data with climate simulations. Such studies will thereby help to minimize a possible misinterpretation of isotope records used for temperature reconstructions during interglacial climates, a topic which has been becoming increasingly focused upon given the growing concerns about future global warming.

While we have performed a preliminary comparison of our simulated δ^{18}O results to the measurements of several ice cores as well as speleothem records, we refrain from performing a more detailed model-data comparison, as this would be beyond the scope of this paper. However, our analysis has demonstrated that we should raise new questions regarding the robustness of δ^{18}O-climate reconstructions; e.g., it should be carefully reassessed if δ^{18}O can be used to reconstruct temperatures during interglacials if the temperature responses are not particularly strong. As we have seen from our study, the temporal δ^{18}O/T quotient might be subject to a large degree of variability.

References

Aggarwal, P. K., U. Romatschke, L. Araguas-Araguas, D. Belachew, F. J. Longstaffe, P. Berg, C. Schumacher, and A. Funk (2016), Proportions of convective and stratiform precipitation revealed in water isotope ratios, *Nat. Geosci.*, *9*(8), 624–629, doi:10.1038/ngeo2739.

Bakker, P., et al. (2013), Last interglacial temperature evolution—A model inter-comparison, *Clim. Past*, *9*(2), 605–619, doi:10.5194/cp-9-605-2013.

Bakker, P., et al. (2014), Temperature trends during the Present and Last Interglacial periods—A multi-model-data comparison, *Quat. Sci. Rev.*, *99*, 224–243, doi:10.1016/j.quascirev.2014.06.031.

Barron, E. J., W. W. Hay, and S. Thompson (1989), The hydrologic cycle: A major variable during earth history, *Palaeogeogr. Palaeoclimatol. Palaeoecol.*, *75*(3), 157–174, doi:10.1016/0031-0182(89)90175-2.

Berger, A., and M. F. Loutre (1991), Insolation values for the climate of the last 10 million years, *Quat. Sci. Rev.*, *10*(4), 297–317, doi:10.1016/0277-3791(91)90033-Q.

Braconnot, P., S. P. Harrison, M. Kageyama, P. J. Bartlein, V. Masson-Delmotte, A. Abe-Ouchi, B. L. Otto-Bliesner, and Y. Zhao (2012), Evaluation of climate models using palaeoclimatic data, *Nat. Clim. Change*, *2*(6), 417–424, doi:10.1038/nclimate1456.

Brocas, W. M., T. Felis, J. C. Obert, P. Gierz, G. Lohmann, D. Scholz, M. Kölling, and S. R. Scheffers (2016), Last interglacial temperature seasonality reconstructed from tropical Atlantic corals, *Earth Planet. Sci. Lett.*, *449*, 418–429.

Brovkin, V., T. Raddatz, C. H. Reick, M. Claussen, and V. Gayler (2009), Global biogeophysical interactions between forest and climate, *Geophys. Res. Lett.*, *36*, L07405, doi:10.1029/2009GL037543.

CAPE Last Interglacial Project Members (2006), Last Interglacial Arctic warmth confirms polar amplification of climate change, *Quat. Sci. Rev.*, *25*(13–14), 1383–1400, doi:10.1016/j.quascirev.2006.01.033.

Capron, E., A. Govin, E. J. Stone, V. Masson-Delmotte, S. Mulitza, B. L. Otto-Bliesner, T. L. Rasmussen, L. C. Sime, C. Waelbroeck, and E. W. Wolff (2014), Temporal and spatial structure of multi-millennial temperature changes at high latitudes during the Last interglacial, *Quat. Sci. Rev.*, *103*, 116–133, doi:10.1016/j.quascirev.2014.08.018.

Cuffey, K. M., and S. J. Marshall (2000), Substantial contribution to sea-level rise during the last interglacial from the Greenland Ice Sheet, *Nature*, *404*(6778), 591–594, doi:10.1038/35007053.

Dansgaard, W. (1964), Stable isotopes in precipitation, *Tellus*, *16*(4), 436–468, doi:10.1111/j.2153-3490.1964.tb00181.x.

Drysdale, R. N., G. Zanchetta, J. C. Hellstrom, A. E. Fallick, J.-X. Zhao, I. Isola, and G. Bruschi (2004), Palaeoclimatic implications of the growth history and stable isotope (δ^{18}O and δ^{13}C) geochemistry of a Middle to Late Pleistocene stalagmite from central-western Italy, *Earth Planet. Sci. Lett.*, *227*(3–4), 215–229, doi:10.1016/j.epsl.2004.09.010.

Drysdale, R. N., J. C. Hellstrom, G. Zanchetta, A. E. Fallick, M. F. S. Goñi, I. Couchoud, J. McDonald, R. Maas, G. Lohmann, and I. Isola (2009), Evidence for obliquity forcing of glacial termination II, *Science*, *325*(5947), 1527–1531, doi:10.1126/science.1170371.

Dutton, A., A. E. Carlson, A. J. Long, G. A. Milne, P. U. Clark, R. DeConto, B. P. Horton, S. Rahmstorf, and M. E. Raymo (2015), Sea-level rise due to polar ice-sheet mass loss during past warm periods, *Science*, *349*(6244), 153, doi:10.1126/science.aaa4019.

EPICA Community Members (2004), Eight glacial cycles from an Antarctic ice core, *Nature*, *429*(6992), 623–628, doi:10.1038/nature02599.

Felis, T., G. Lohmann, H. Kuhnert, S. J. Lorenz, D. Scholz, J. Pätzold, S. A. Al-Rousan, and S. M. Al-Moghrabi (2004), Increased seasonality in Middle East temperatures during the last interglacial period, *Nature*, *429*(6988), 164–168, doi:10.1038/nature02546.

Felis, T., C. Giry, D. Scholz, G. Lohmann, M. Pfeiffer, J. Pätzold, M. Kölling, and S. R. Scheffers (2015), Tropical Atlantic temperature seasonality at the end of the last interglacial, *Nat. Commun.*, *6*, 6159, doi:10.1038/ncomms7159.

Haese, B., M. Werner, and G. Lohmann (2013), Stable water isotopes in the coupled atmosphere-land surface model ECHAM5-JSBACH, *Geosci. Model Dev.*, *6*(5), 1463–1480, doi:10.5194/gmd-6-1463-2013.

Haywood, A. M., et al. (2013), Large-scale features of Pliocene climate: Results from the Pliocene Model Intercomparison Project, *Clim. Past*, *9*(1), 191–209, doi:10.5194/cp-9-191-2013.

Herold, M., and G. Lohmann (2009), Eemian tropical and subtropical African moisture transport: An isotope modelling study, *Clim. Dyn.*, *33*(7–8), 1075–1088, doi:10.1007/s00382-008-0515-2.

Holloway, M. D., L. C. Sime, J. S. Singarayer, J. C. Tindall, P. Bunch, and P. J. Valdes (2016), Antarctic last interglacial isotope peak in response to sea ice retreat not ice-sheet collapse, *Nat. Commun.*, *7*, 12293, doi:10.1038/ncomms12293.

IAEA/WMO (2017), *Global Network of Isotopes in Precipitation*, The GNIP Database, Vienna, Austria. [Available at http://www.iaea.org/water.]

Jungclaus, J. H., N. Keenlyside, M. Botzet, H. Haak, J. J. Luo, M. Latif, J. Marotzke, U. Mikolajewicz, and E. Roeckner (2006), Ocean circulation and tropical variability in the coupled model ECHAM5/MPI-OM, *J. Clim.*, *19*(16), 3952–3972, doi:10.1175/JCLI3827.1.

Kim, S.-T., C. Hillaire-Marcel, and A. Mucci (2006), Mechanisms of equilibrium and kinetic oxygen isotope effects in synthetic aragonite at 25°C, *Geochim. Cosmochim. Acta*, *70*(23), 5790–5801, doi:10.1016/j.gca.2006.08.003.

Knutti, R., R. Furrer, C. Tebaldi, J. Cermak, and G. A. Meehl (2010), Challenges in combining projections from multiple climate models, *J. Clim.*, *23*(10), 2739–2758, doi:10.1175/2009JCLI3361.1.

Kopp, R. E., F. J. Simons, J. X. Mitrovica, A. C. Maloof, and M. Oppenheimer (2009), Probabilistic assessment of sea level during the last interglacial stage, *Nature*, *462*(7275), 863–867, doi:10.1038/nature08686.

Lee, J. E., I. Fung, D. J. DePaolo, and C. C. Henning (2007), Analysis of the global distribution of water isotopes using the NCAR atmospheric general circulation model, *J. Geophys. Res.*, *112*, D16306, doi:10.1029/2006JD007657.

Lohmann, G., M. Pfeiffer, T. Laepple, G. Leduc, and J. H. Kim (2013a), A model–data comparison of the Holocene global sea surface temperature evolution, *Clim. Past*, *9*(4), 1807–1839, doi:10.5194/cpd-8-1005-2012.

Lohmann, G., A. Wackerbarth, P. Langebroek, M. Werner, J. Fohlmeister, D. Scholz, and A. Mangini (2013b), Simulated European stalagmite record and its relation to a quasi-decadal climate mode, *Clim. Past*, *9*, 89–98, doi:10.5194/cp-9-89-2013.

Loulergue, L., A. Schilt, R. Spahni, V. Masson-Delmotte, T. Blunier, B. Lemieux, J. M. Barnola, D. Raynaud, T. F. Stocker, and J. Chappellaz (2008), Orbital and millennial-scale features of atmospheric CH_4 over the past 800,000 years, *Nature*, *453*(7193), 383–386, doi:10.1038/nature06950.

Lunt, D. J., et al. (2013), A multi-model assessment of last interglacial temperatures, *Clim. Past*, *9*(2), 699–717, doi:10.5194/cp-9-699-2013.

Lüthi, D., et al. (2008), High-resolution carbon dioxide concentration record 650,000–800,000 years before present, *Nature*, *453*(7193), 379–382, doi:10.1038/nature06949.

Masson-Delmotte, V., et al. (2008), A review of Antarctic surface snow isotopic composition: Observations, atmospheric circulation, and isotopic modeling, *J. Clim.*, *21*(13), 3359–3387, doi:10.1175/2007JCLI2139.1.

Masson-Delmotte, V., D. Buiron, and A. Ekaykin (2010), A comparison of the present and last interglacial periods in six Antarctic ice cores, *Clim. Past*, *7*, 397–423.

Masson-Delmotte, V., et al. (2011), Sensitivity of interglacial Greenland temperature and delta 18O: Ice core data, orbital and increased CO_2 climate simulations, *Clim. Past*, *7*(3), 1041–1059, doi:10.5194/cp-7-1041-2011.

NEEM Community Members (2013), Eemian interglacial reconstructed from a Greenland folded ice core, *Nature*, *493*(7433), 489–494, doi:10.1038/nature11789.

O'Leary, M. J., P. J. Hearty, W. G. Thompson, M. E. Raymo, J. X. Mitrovica, and J. M. Webster (2013), Ice sheet collapse following a prolonged period of stable sea level during the last interglacial, *Nat. Geosci.*, *6*(9), 796–800.

Otto-Bliesner, B. L., N. Rosenbloom, E. J. Stone, N. P. McKay, D. J. Lunt, E. C. Brady, and J. T. Overpeck (2013), How warm was the last interglacial? New model-data comparisons, *Philos. Trans. R. Soc. A*, *371*(2001), 20130097, doi:10.1098/rsta.2013.0097.

Pfeiffer, M., and G. Lohmann (2016), Greenland Ice Sheet influence on Last Interglacial climate: Global sensitivity studies performed with an atmosphere–ocean general circulation model, *Clim. Past*, *12*(6), 1313–1338, doi:10.5194/cpd-11-933-2015.

Risi, C., S. Bony, F. Vimeux, and J. Jouzel (2010), Water-stable isotopes in the LMDZ4 general circulation model: Model evaluation for present-day and past climates and applications to climatic interpretations of tropical isotopic records, *J. Geophys. Res.*, *115*, D12118, doi:10.1029/2009JD013255.

Roeckner, E., R. Brokopf, M. Esch, M. Giorgetta, S. Hagemann, L. Kornblueh, E. Manzini, U. Schlese, and U. Schulzweida (2006), Sensitivity of simulated climate to horizontal and vertical resolution in the ECHAM5 atmosphere model, *J. Clim.*, *19*(16), 3771–3791, doi:10.1175/JCLI3824.1.

Rozanski, K., L. Araguas-Araguas, and R. Gonfiantini (1992), Relation between long-term trends of oxygen-18 isotope composition of precipitation and climate, *Science*, *258*(5084), 981–5, doi:10.1126/science.258.5084.981.

Sime, L. C., J. C. Tindall, E. W. Wolff, W. M. Connolley, and P. J. Valdes (2008), Antarctic isotopic thermometer during a CO_2 forced warming event, *J. Geophys. Res.*, *113*, D24119, doi:10.1029/2008JD010395.

Sime, L. C., E. W. Wolff, K. I. C. Oliver, and J. C. Tindall (2009), Evidence for warmer interglacials in East Antarctic ice cores, *Nature*, *462*(7271), 342–345, doi:10.1038/nature08564.

Sime, L. C., C. Risi, J. C. Tindall, J. Sjolte, E. W. Wolff, V. Masson-Delmotte, and E. Capron (2013), Warm climate isotopic simulations: What do we learn about interglacial signals in Greenland ice cores?, *Quat. Sci. Rev.*, *67*, 59–80, doi:10.1016/j.quascirev.2013.01.009.

Sjolte, J., and G. Hoffmann (2014), Modelling stable water isotopes in monsoon precipitation during the previous interglacial, *Quat. Sci. Rev.*, *85*, 119–135, doi:10.1016/j.quascirev.2013.12.006.

Sjolte, J., G. Hoffmann, S. J. Johnsen, B. M. Vinther, V. Masson-Delmotte, and C. Sturm (2011), Modeling the water isotopes in Greenland precipitation 1959–2001 with the meso-scale model REMO-iso, *J. Geophys. Res.*, *116*, D18105, doi:10.1029/2010JD015287.

Spahni, R., et al. (2005), Atmospheric methane and nitrous oxide of the late Pleistocene from Antarctic ice cores, *Science*, *310*(5752), 1317–1321, doi:10.1126/science.1120132.

Steig, E. J., P. M. Grootes, and M. Stuiver (1994), Seasonal precipitation timing and ice core records, *Science*, *266*(5192), 1885–1886.

Stepanek, C., and G. Lohmann (2012), Modelling mid-Pliocene climate with COSMOS, *Geosci. Model Dev.*, *5*(5), 1221–1243, doi:10.5194/gmd-5-1221-2012.

Sutter, J., P. Gierz, K. Grosfeld, M. Thoma, and G. Lohmann (2016), Ocean temperature thresholds for Last Interglacial West Antarctic Ice Sheet collapse, *Geophys. Res. Lett.*, *43*, 2675–2682, doi:10.1002/2016GL067818.

Tindall, J. C., and A. M. Haywood (2015), Modeling oxygen isotopes in the Pliocene: Large-scale features over the land and ocean, *Paleoceanography*, *30*, 1183–1201, doi:10.1002/2014PA002774.

Trenberth, K. E., A. Dai, R. M. Rasmussen, and D. B. Parsons (2003), The changing character of precipitation, *Bull. Am. Meteorol. Soc.*, *84*(9), 1205–1217, doi:10.1175/BAMS-84-9-1205.

Werner, M., P. M. Langebroek, T. Carlsen, M. Herold, and G. Lohmann (2011), Stable water isotopes in the ECHAM5 general circulation model: Toward high-resolution isotope modeling on a global scale, *J. Geophys. Res.*, *116*, D15109, doi:10.1029/2011JD015681.

Werner, M., B. Haese, X. Xu, X. Zhang, M. Butzin, and G. Lohmann (2016), Glacial–interglacial changes in $H_2^{18}O$, HDO and deuterium excess—Results from the fully coupled ECHAM5/MPI-OM Earth system model, *Geosci. Model Dev.*, *9*(2), 647–670, doi:10.5194/gmdd-8-8835-2015.

Wild, M., J. Grieser, and C. Schär (2008), Combined surface solar brightening and increasing greenhouse effect support recent intensification of the global land-based hydrological cycle, *Geophys. Res. Lett.*, *35*, L17706, doi:10.1029/2008GL034842.

Xu, X., M. Werner, M. Butzin, and G. Lohmann (2012), Water isotope variations in the global ocean model MPI-OM, *Geosci. Model Dev.*, *5*(3), 809–818, doi:10.5194/gmd-5-809-2012.